Trapping and Moving Atoms on Surfaces

Robert J. Celotta[*] and Joseph A. Stroscio
Electron Physics Group, National Institute of Standards and Technology,
Gaithersburg, Maryland, 20899-8412

Abstract

We have used a scanning tunneling microscope to laterally reposition a single cobalt atom adsorbed on the (111) face of a copper crystal. We find that the atom follows a complex path determined by the trapping potential of the STM tip, the effects of vibrational heating from inelastic electron scattering, and the overall potential landscape of the crystal surface. The atom's dynamical response produces the classic signature of a random two-state fluctuator, permits the acquisition of a binding site image of the surface, and suggests a methodology for atom-based measurements of nanostructures.

I. Introduction

We credit the Greek civilization with giving us the first atomic theory over twenty-four centuries ago. Democritus (460-370 BC) reasoned that by constantly dividing a pure substance, we would eventually reach the stage where the products of any further division would no longer have the properties of the initial substance. He called the smallest indivisible particle an atom, following from the Greek word for indivisible. Now, at the

---

[*] I was an early graduate student of Benjamin Bederson. Coincidentally, our first joint publication (Levine, Celotta, and Bederson, 1968) was similar to the research reported here in that we made our measurement by controlling the motion of a single atom. During the many years that separate these two works, I have constantly found myself in Ben's debt for what he taught me, either directly or by example. I have greatly benefited from the knowledge and skills he passed on, the importance he placed on communicating well the results of ones research, and the enthusiasm for science he exuded. For these, and many other contributions, I extend my admiration and appreciation.

start of the twenty-first century, the burgeoning fields of nanoscale science and nanotechnology have arisen from the realization that particles of pure substances with lengths up to a few hundred atoms in each dimension can have dramatically different properties from those of the bulk material. These new properties exist because of three different characteristic phenomena found in nanostructures: coherence, confinement, and coordination. Within nanostructures, electrons frequently move with phase coherence and are therefore able to exhibit interference effects. The electron dephasing length can be long enough that the electron can repeatedly sense the boundaries of the nanostructure; such electron confinement gives rise to new electronic states. Finally, as a nanostructure's size decreases, a larger fraction of the atoms are positioned at the surfaces, edges, or corners rather than in bulk locations and exhibit new properties, such as increased reactivity, due to their different coordination.

A core motivation of nanoscale science is the purposeful engineering of new materials properties; these properties reflect, for example, the new electronic structure created by modifying physical structure on the nanoscale. In the ideal case, we would put each atom exactly where we wanted it to be (Feynman, 1960) to take full advantage of the opportunities afforded us to custom tailor materials properties. Research on the manipulation of single atoms using Scanning Tunneling Microscopy (STM) is an attempt to discover just how close to the ideal we can come.

A wide variety of mechanisms (Avouris, 1995) are possible to explain how an STM tip is able to move an adsorbate atom, or adatom, laterally along a surface. It is useful to

separate them into interactions that cause the adatom to be attracted to the tip and those that simply enhance its mobility. When the tip is brought in close proximity of the surface, an attractive Van der Waals interaction can be expected between the adatom and the atoms terminating the tip; eventually, at smaller distances, chemical bonding begins. Since the energy barrier to surface diffusion on metals is only a fraction of the energy with which the adatom is bound to the surface, the Van der Waals interaction might suffice to move an adatom weakly physisorbed to the surface. A more strongly bound chemisorbed adatom may require a stronger bond between adatom and tip for repositioning to occur. Additional forces on the adatom can arise because of the presence of the inhomogeneous electric field produced by the STM tip. There may be an electric dipole moment at the adatom caused by charge transfer with the surface resulting from the adatom-substrate bond or the tip's electric field may induce an electric dipole moment via the adatom's polarizability. In either case, a lateral force can result from the interaction between the overall electric dipole moment and the tip's inhomogeneous electric field.

The voltage between the tip and the surface and the electron tunneling current flowing could also have important effects that could aid adatom mobility. The electron current may excite the vibrational states of the adatom-surface potential through inelastic electron scattering. The voltage may play a role by exceeding thresholds necessary to open additional channels leading to enhanced diffusion. Moreover, the presence of a high, tip-generated electric field may affect the strength of the adsorbate bonding directly, in the limiting case producing electric field induced desorption.

In this report, we will attempt to describe in detail how a Co adatom is moved laterally across a Cu(111) surface using an STM (Stroscio and Celotta, 2004). The choice of the Co/Cu(111) system was based on other experiments that we had in mind and not because atom manipulation is in any way novel in this system. We will find that the adatom's motion is complex and dynamic; it is best understood in terms of a tip derived scannable atom trap that constrains the adatom to a small lateral region beneath the tip. We begin by very briefly describing some of the successes of atom manipulation, move on to describing our experimental method, results, and conclusions, and end with a look at possible future trends.

II. Moving Atoms

A. Background

The early work on atom manipulation showed that the STM could be used to position individual atoms or groups of atoms on a surface (Stroscio and Eigler, 1991). In the ground breaking work of Eigler (1990), xenon atoms were physisorbed on a Ni(110) surface at a temperature of 4K and moved through an interaction with the STM tip thought to consist of a combination of Van der Waals and electrostatic interactions. It was then demonstrated (Whitman et al., 1991) that Cs atoms deposited on the (110) surface of GaAs form long zigzag chains of atoms beneath the STM tip as a result of a pulse in the voltage applied between the tip and a room temperature surface. The authors ascribe the mechanism to electric field induced diffusion.

In the decade that followed, great strides were made in learning to use scanning tunneling microscopes to manipulate individual atoms and molecules adsorbed on surfaces (Gimzewski and Joachim, 1999). One and two-dimensional nanostructures were constructed with both closely and sparsely packed atoms. Electron scattering boundaries made of adatoms were used to confine surface state electrons and produce complex electron standing wave structures (Crommie et al., 1993) and project the electronic structure of a single atom (Manoharan et al., 2000).

Progress was also made in our understanding of the atomic manipulation process through STM measurements (Bartels et al., 1997; Hla et al., 2003), and simulations (Kuhnle et al., 2002). In many instances, the tip-adatom interaction was thought of as a tunable chemical bond. Lacking in this progress was an appreciation of the roles played by dynamical and inelastic electron scattering processes in lateral atom manipulation. Dynamical processes driven by inelastic electron scattering have been investigated in connection with vertical atom manipulation (Eigler, 1991) and molecular manipulation (Stipe et al., 1998; Ho, 2002).

B. Experimental System

Briefly stated, scanning tunneling microscopy (Binnig et al., 1983; Stroscio and Kaiser, 1993) is practiced by rastering a metal tip, which has been prepared to terminate in a fine point (ideally a single atom), a few Ångstroms above a conducting surface. A small bias voltage between tip and sample is sufficient to produce a current of electrons across the few Ångstrom vacuum gap as a consequence of electron tunneling. Because the metal-

vacuum-metal tunneling probability varies exponentially with the distance, small changes in the distance between tip and sample correspond to large changes in the tunneling current, i.e., the current changes by a factor of ten for an approximately 1 Å change in distance. A constant tip height above the surface is maintained to high precision by servo controlling the tunneling current using piezoelectric transducers to adjust the tip height. The surface described by the tip motion during the raster scan of an area is taken to be a "topograph" of the surface.

We studied the movement of Co atoms on a Cu(111) substrate in a low-temperature STM (LT-STM) of our own design. This instrument is capable of operating with a sample held at a temperature within the range of 2.3 K – 4.3 K in an ultra-high-vacuum. Sample preparation facilities allow for preparation of clean flat substrates using ion sputtering and annealing. Reflection high-energy electron diffraction (RHEED) is used to monitor the surface preparation process. A Field Ion Microscope (FIM) is also attached to the LT-STM and is used to clean, by field evaporation, the Ir STM tips used in this work, as well as to image directly the atomic structure at the tip termination.

STM measurements in general and the measurement of the atom dynamics during atom manipulation are very sensitive to mechanical and electronic noise sources. For this reason, all sources of mechanical and electrical noise must be minimized. The LT-STM resides in an acoustically and electrically shielded room and is vibrationally isolated from the room floor by a series of three isolation systems.

Cu(111) top view
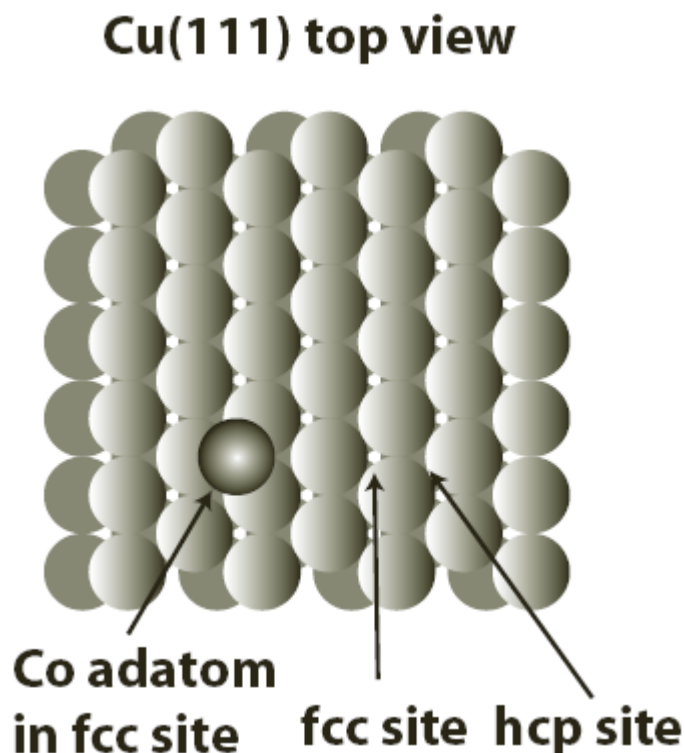

Co adatom in fcc site   fcc site   hcp site

Figure 1. Two layers of a Cu(111) crystal face shown with a Co atom residing in its natural fcc site. The labeled fcc and hcp hollow sites differ by presence or absence of a Cu atom in the second layer (Stroscio and Celotta, 2004).

C. Co/Cu(111)

Bulk copper has a face centered cubic crystal structure. Figure 1 schematically shows the top two surface layers of the (111) crystal face of a Cu crystal. The face-centered-cubic site, labeled fcc, is the site that would be filled during the next layer of Cu growth. The similar 3-fold hollow hexagonal-close-packed (hcp) site differs from the fcc site by having an atom directly under it two layers down. The fcc site is the preferred site for a single Co atom on Cu(111) as depicted in Figure 1, based on our measurements of Cu and Co mixtures (to be published), which agree with theoretical calculations (Tsivlin et al., 2003).

Typically an STM topographic image of a Co atom atop a Cu(111) surface does not

reveal the lattice structure present in Figure 1. In Figure 2, we see an STM topography

image of a single Co atom on Cu(111) and its immediate surroundings. The modulations

in the background do not reveal the locations of the Cu ion cores but, instead, originate as

a consequence of interference in the scattering of surface state electrons. The electron

density of states for this close-packed Cu surface is sufficiently smooth that the

underlying lattice structure is not typically observable. Even in a system where the

surface corrugation is routinely measurable (Stroscio et al., 1992), the difference between

an fcc and hcp site is not detectable in an STM topographic image. As shown below,

using atom manipulation in a new type of imaging mode, we are able to image both fcc

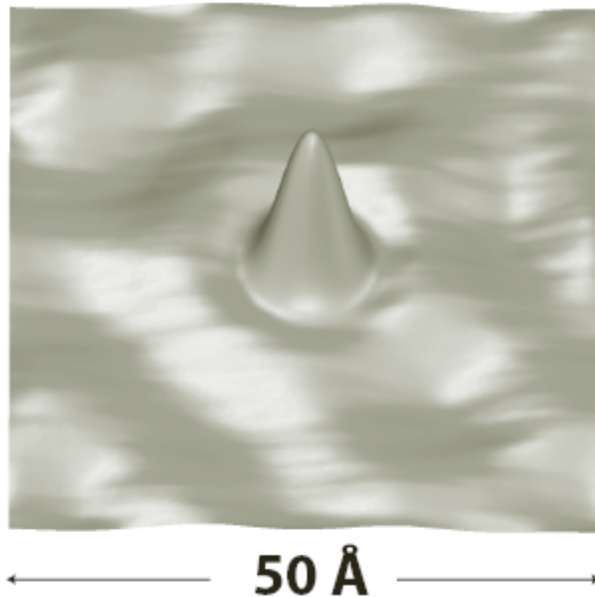and hcp sites with different contrast.

Figure 2. STM topographic image of a single Co atom adsorbed on a Cu(111) substrate, shown in a light shaded view. The wave like undulations seen on the substrate is an interference pattern arising from the scattering of a 2-dimensional electron surface state from adsorbate atoms. Tunnel current 1 nA, sample bias 10 mV, T = 2.3 K, height range 80 pm.

D. The Atom Manipulation Process

The STM plays a dual role in atom manipulation; it moves the atoms and provides images of the atom arrangement. Indeed, the ability to both image and move atoms depends on a series of energy inequivalences. First, to have a stable atom arrangement the energy needed to surmount the diffusion barrier to lateral motion must be high compared to that available from the thermal bath at the substrate temperature. Second, the tip-adatom interaction during *imaging* must be low enough so that the adatoms do not move. Third, the tip-adatom interaction during *moving* must be sufficient to exceed the local barriers to lateral motion. Finally, the tip-adatom interaction energy must not be great enough to transfer the adatom from the surface to the tip. Fortunately, the substrate temperature, tip height, and tunneling current are available parameters that can be used to adjust these important energies to allow both imaging and manipulation.

Generally, we characterize the tip-height by the tunneling gap impedance. While imaging, the tunneling gap impedance for Co/Cu(111) is typically 10 MΩ, derived from a bias voltage (the potential of the tip relative to the sample) of -10 mV and an operating current of 1 nA. In order to move a Co atom, an impedance of 80 k Ω (-8 mV, 100 nA) is typically used. The "move" process begins after the general area is imaged at the imaging impedance. Then, with the STM set to the imaging impedance, the tip is repositioned to a point directly above the atom to be moved. The impedance is then changed to the move impedance, the tip moves downward to the adatom as the STM servo satisfies the demand for a higher current, and the tip is moved laterally at that impedance to the desired spot. Finally, the impedance is changed to the imaging

impedance, the tip moves upward away from the adatom, leaving the adatom in its new location. An image may be taken to verify that the move was accomplished as expected. In practice, there are two difficulties involved in using this process: A precise map of the stable destination sites is required if an exact final geometry is desired and the optimal move impedance needs to be determined. We will defer the site determination problem until the next section. A search for the optimal move impedance can be executed by programming the STM controller to repeatedly attempt to move an adatom back and forth between neighboring sites while keeping track of the success rate. For the Ag/Ag(111) system, Hla et al. (2003) used this method. They found a clear threshold current of about 200 nA for the -45 mV bias potential used. By repeating this process for different bias voltages, Hla et al. found that the impedance, with a threshold value of 210 kΩ, was the key parameter. We find a similar threshold impedance of 200 kΩ for Co on Cu(111).

III. Atom Dynamics

A. STM Observation of Atom Motion

As has been well demonstrated (Bartels et al., 1997), a great deal of information about the motion of an adsorbate atom during manipulation is contained in a plot of the measured tip height versus distance along the crystal surface. In Figure 3, we show a schematic depiction of substrate, adatom, and tip, along with an actual measurement of the tip height as the tip traces along the crystal surface. Also shown is the attractive force between tip and adatom. As the tip moves to the right, the adatom appears to remain in its fcc binding site and the tip traces over the atom in a smooth arc. Next, we see a narrow peak with a sharp vertical onset at approximately the hcp binding site of the Cu

10

substrate. Finally, we see that the tip moves in toward the surface at the position of a Cu atom in the substrate. This pattern repeats for each unit cell of the underlying crystal lattice. Were the direction of tip motion along the surface arbitrary, and not along a crystal symmetry direction as shown here, a much more complex tip height trace would have been measured.
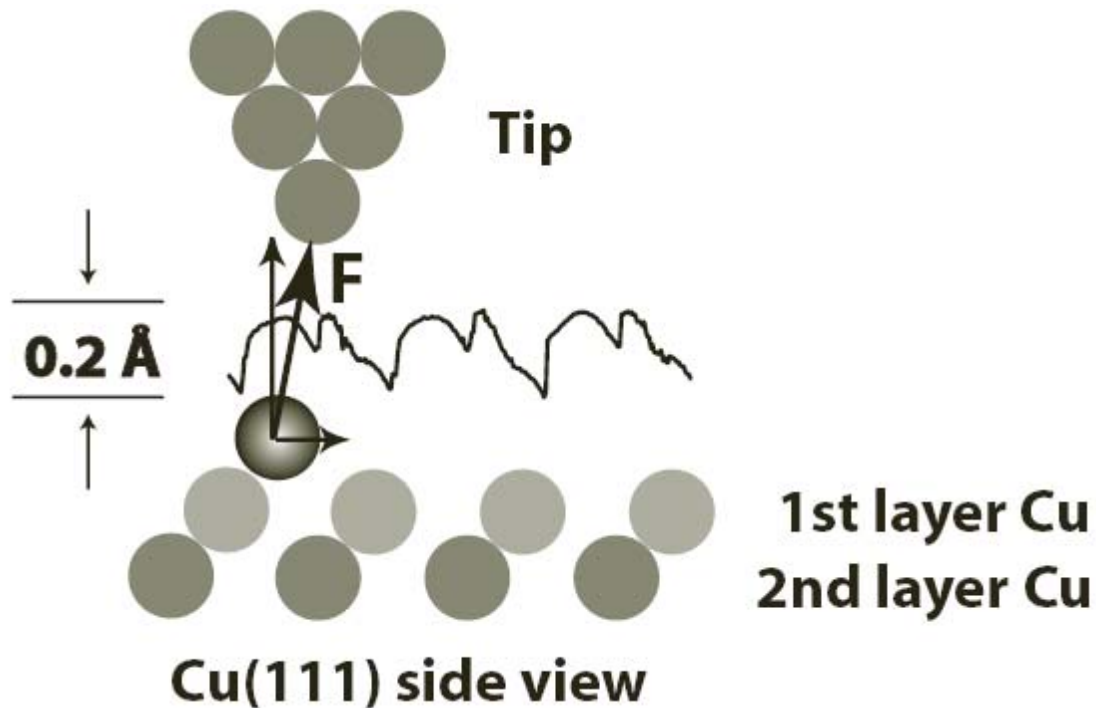

Figure 3. Side view of tip–adatom interaction showing the Co atom in the fcc site and the top two layers of the Cu(111) crystal. The force attracting the adatom to the tip is indicated. A trace is shown of the measured tip height as the Co atom is moved along the surface.

In order to get a more complete picture of the atom motion across the surface, we raster scanned the surface, exactly as one would to obtain an STM topograph, except in this case with a Co adatom captured beneath the tip. This is possible by acquiring a full image at the move impedance value of 100 kΩ. The result, which we refer to as a manipulated atom image, appears in Figure 4A. This image shows a substrate that appears to be very different from that seen surrounding a Co atom in Figure 2, yet each

image reflects the tip height of an STM tip moving over the same sample and both tips are believed to be terminated in a single atom. We see what look like single atoms in the image of Figure 4A and they appear to have the ordering and spacing of the Cu(111) lattice. Surrounding each atom-like feature, three white triangles appear giving rise to an image very similar to the schematic depiction of the Cu(111) crystal structure presented in Figure 1. Yet, the three-fold symmetry surrounding each top-layer Cu atom in Figure 1 is due to presence or absence of a Cu atom in the first subsurface layer. It would be remarkable to go from a normal atomic resolution STM topograph, which is not even sensitive to the top layer structure, i.e., Figure 2, to one that clearly reflects the structure of a subsurface layer as well!

Another curious aspect of the data shown in Figure 4A is that the white triangular structure appears to be "noisier" than the adjacent structures. The maximum values of tip height recorded in the white triangles are approximately the same as at the centers of the round, ball like structures, but there are considerable downward fluctuations in the triangles that appear as black pixels. We were also aware of these unusual "noisy" areas because we monitored the measured tunneling current in real time by connecting the signal through a high bandwidth channel to a laboratory audio system. We heard perfectly periodic "noise" bursts as the tip scanned the Cu(111) surface, as can be seen in Figure 4B.

In order to understand what the image in Figure 4A represents, we focus on the effect of the tip on the potentials that lie along the horizontal scan line indicated there. Figure 5A

shows the fcc and hcp potential wells and the barrier between them. The fcc potential is

deeper and consequently, in the absence of any tip-adatom interaction, the Co atom will

almost always be found there at the temperatures used in these experiments. In Figure

5B, we schematically represent the tip-adatom attraction as a potential centered on the tip

position which has the effect of lowering the potential well beneath the tip. As seen in

Figure 5C, owing to the addition of a strong tip-adatom interaction, the hcp site potential

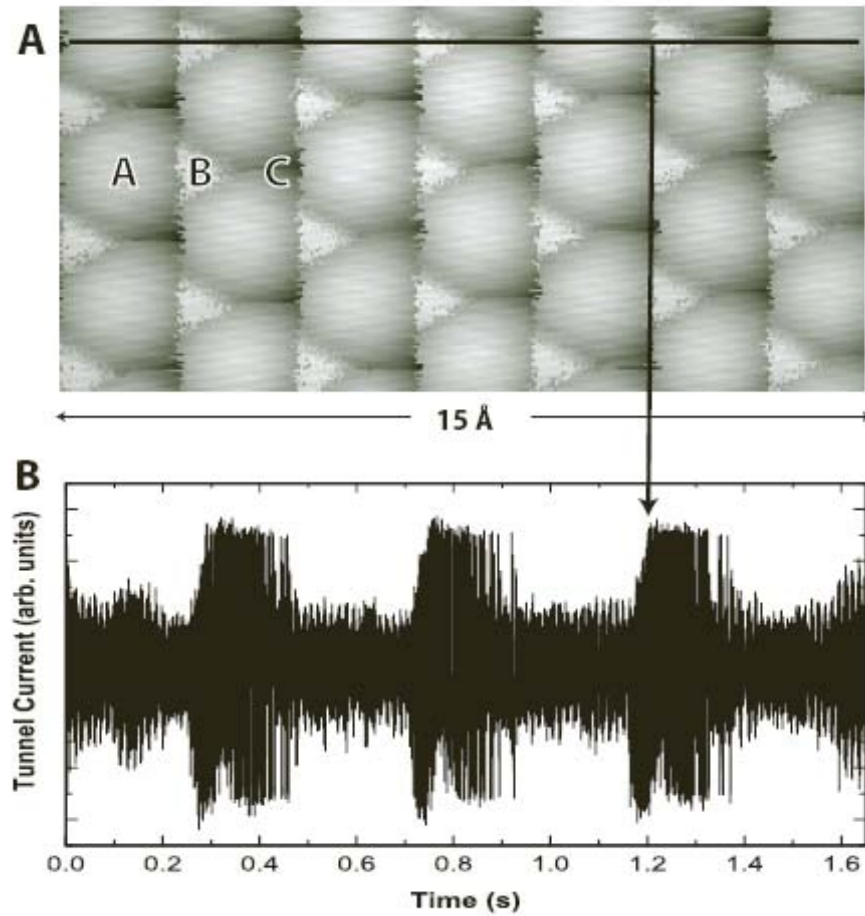has been depressed sufficiently to become the favored binding site.

Figure 4. (A) Manipulated atom image of Co over Cu(111) surface. The three different features labeled A, B, and C are discussed in the text. Tunnel current 50 nA, sample bias −5 mV, T = 4.3 K. (B) A time sequence trace of the tunnel current corresponding to the horizontal black line in A with a vertical arrow highlighting the onset of a noise burst coincident with the tip entering region B (Stroscio and Celotta, 2004).

Returning to the image in Figure 4A, we can understand the sites probed as the Co atom is moved by the tip scanning along the indicated horizontal scan line with the help of Figures 3 and 5. The first ball-like object on the left (at site A) is the Co atom residing in a Cu fcc site. This is the lowest energy state predicted by Tsivlin et al. (2003). In the image of Figure 4A, the tip is measuring the height contour of an adsorbed Co atom. This can also be seen in Figure 3. When the tip has scanned to a position over site B, an hcp binding site, we see a "noisy" white triangle in Figure 4A. This can be understood as follows: The tip-adatom potential is sufficient in this case to depress the potential at the hcp site to the point that the adatom will sometimes leave the fcc site and reside at the hcp site. When the Co atom is at the hcp site, the measured tip height is the same as when the tip is above the Co atom when the atom is at the fcc site. However, the Co atom can jump continuously between the two sites, and at this impedance, spends most of its time at the fcc site. That is why it appears as an adsorbed atom at the fcc site and gives rise to what appear to be fluctuations at the hcp site. Site C is a binding site that corresponds to a Co atom bound directly on top of a Cu atom. This is a low point in the image, which indicates that the atom moves to the side of the tip, within the capture range of the tip-adatom potential, and presumably visits the adjacent fcc sites that appear as round balls in Figure 4A. Hence, the Co atom's motion across the three sites labeled in Figure 4A can be explained by having the tip-adatom potential modify the local potential landscape in such a way that the Co atom first pauses at its favored fcc binding site, is then intermittently attracted to the adjacent hcp site, and then visits a more stable adjacent fcc site when the tip attempts to position it over a site on top a Cu atom. Because the structures present in this image, obtained by rastering a Co atom across a Cu(111)

surface, correspond to three different possible binding sites for the Co atom, we refer to this manipulated atom image as a *binding site image* of Co/Cu(111). Such an image offers remarkable detail as opposed to the undetectably small variations in topography available from a conventional topographic image of a Cu(111) surface.
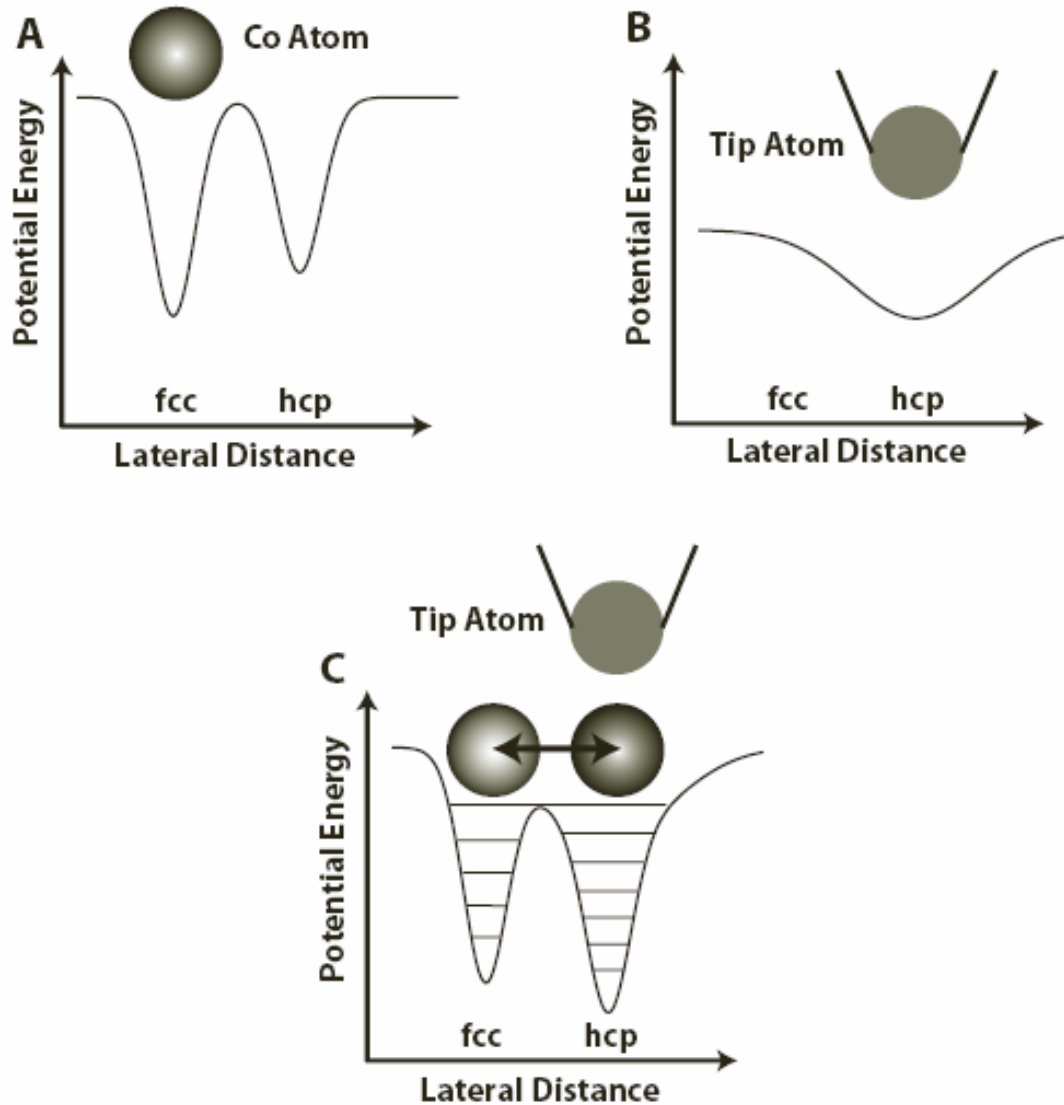

Figure 5. (A) A schematic depiction of the potential that exists along the horizontal line of tip travel drawn in Fig. 4A showing the Co adatom resting in the fcc binding site. (B) A schematic depiction of the local potential minimum beneath the tip caused by the tip–adatom interaction. (C) The full potential when the tip is located above the hcp site showing that the hcp site has become the energetically favored site.

It is important to keep in mind that even though the image of Figure 4A bears an uncanny resemblance to the Cu(111) surface structure illustrated in Figure 1, the ball-like objects in Figure 4A are not Cu substrate atoms, but instead the multiple imaging of a single manipulated Co atom at its favored fcc binding sites.

B. An Ideal Two-State Fluctuator

The time sequence shown in Figure 4b shows what appears to be an increase in the noise in the tunneling current as the tip traces through the location of an hcp site. In order to better study the source and characteristics of this noise, the scan was interrupted, and measurements of the tunneling current were made while the tip was stationary over the hcp site. Figure 6A shows a portion of a binding site image with three tip locations (B, C, and D) marked. For these measurements, the tip images the surface with a Co atom trapped beneath it and pauses at each of the three marked positions. At each of these precisely located positions, the servomechanism maintaining the tip height is turned off and the tunneling current is monitored continuously using a relatively high bandwidth system. The time trace shown in Figure 6B, corresponding to location B at the hcp site that is nearest to fcc site #1, shows a system that is switching between two states. The higher current state corresponds to the Co atom occupying the hcp state, while the more frequent, lower current state records the Co atom occupying the near by and more stable fcc#1 state. A histogram of the tunneling current values is shown to the right. When the tip is moved to position C, closer to the center of the hcp site, the time sequence data in Figure 6C displays a high current value consistent with the hcp site assignment and three different lower current values that we can identify as corresponding to the fcc#1, fcc#2,

and fcc#3 sites. Here the Co atom is jumping back and forth between the hcp site under the tip and all three adjacent fcc sites. Note that we never observe it make a transition between fcc sites. Finally, at location D, furthest from the fcc#1 site, we again observe a two level system, this time involving the fcc#2 site. From this data, we learn that for three tip locations above the hcp site the Co atom is jumping back and forth between the hcp site and the nearby fcc sites. For the tip-adatom interaction used, the atom is spending the majority of its time in fcc sites. The distribution of times spent in either
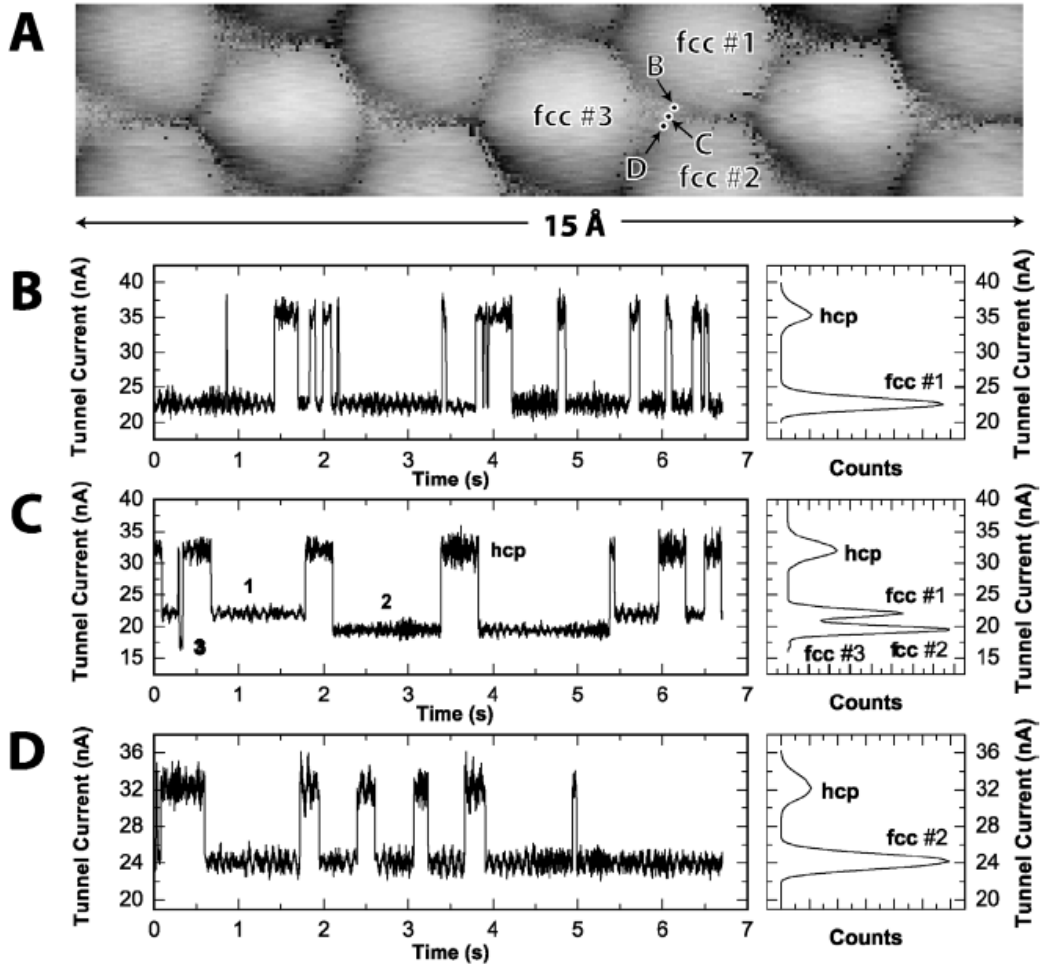

Figure 6. (A) Co manipulated atom image on Cu(111). Tunnel current 100 nA, sample bias 11.0 mV, T = 2.3 K. (B–D) Tunnel current vs. time measurements recorded at the positions indicated by the corresponding spots in A, all near the hcp site. Sample bias 3.3 mV. The corresponding histograms of the current distributions are shown to the right of each graph in B–D.

site, before making transitions to the other site, varies depending on the strength of the tip-adatom interaction.

By analyzing a different time sequence of events in greater detail, it is possible to determine the distribution of residence times for the atom at each site. Figure 7A shows a portion of a time trace taken for an impedance where the atom spends most of its time above the hcp site, as indicated in Figure 7B. Note that the time scale is much shorter than previously shown as the transitions are occurring more rapidly for these conditions.
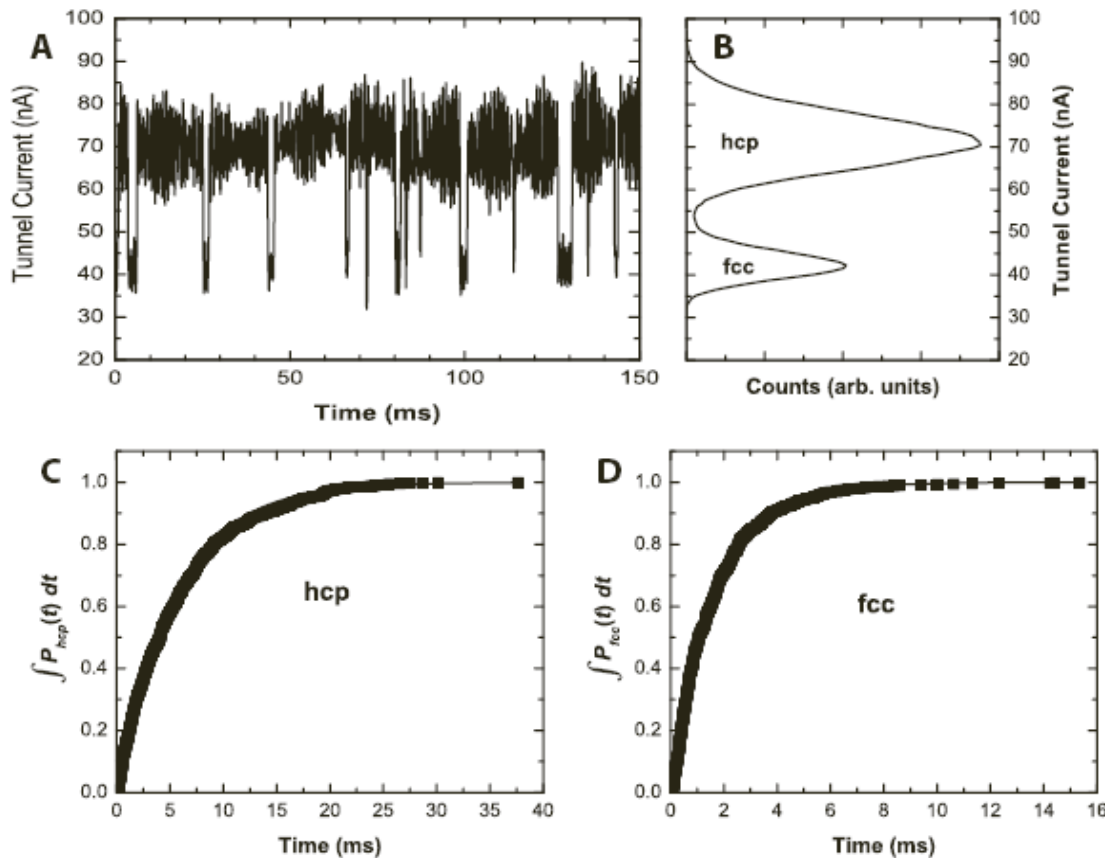

Figure 7. **(A) Tunnel current vs. time measurement showing two-state random telegraph noise near the hcp site recorded during a Co manipulated atom image on Cu(111). Sample bias during current measurement is 8.4 mV, T = 2.3 K. (B) Corresponding tunnel current histogram distribution. (C–D) Symbols show integrated residence time distribution for the hcp and fcc states obtained by measuring the hcp to fcc transitions and residence times in each state for the time sequence data shown partially in A; solid lines fit to the exponential distributions.**

18

Using a long data record, accumulated over as much as ten minutes (during which period, drifts of the tip relative to the sample were less than 2 pm in all directions), it was possible to record the timing of each transition and study the distributions of residence times in each of the two sites. Figures 7C and D show the integrated probability of residence times in the hcp and fcc states, respectively. Since the residence time data agree well with an exponential decay law, we can summarize all of these observations with just two transition rates, i.e., 184.6 ± 3.0 Hz and 568.2 ± 6.8 Hz for leaving the hcp and fcc states respectively.

The observed exponential residence time distributions are characteristic of a two-state discrete Markov process. Such processes occur when the probability of making a transition to the next state is independent of the systems past history. The bistable nature of the tunneling current provides an excellent example of a random two-state fluctuator where the source of the current fluctuations is readily identifiable. A distribution of such two state fluctuators is thought to play a central role in explaining the origin of the ubiquitous 1/f noise found in many electronic devices (Weissman, 1988).

C. Transition Rate Observations

Now that we can characterize the Co atom dynamics by two transition rates, i.e., the rates out of the fcc and hcp sites, it is of interest to see how the dynamics depends on the tunneling current. To do this the tip is again positioned over the hcp site, the tip height servo is turned off, and the time history of the tunneling current is recorded for a series of bias voltages. The transition rates for leaving the hcp and fcc sites are extracted from the

19

data and are shown in Figure 8. Both transition rates are independent of bias voltage up to a bias of about -5 mV where they increase rapidly with increasing negative bias. Very similar results are observed for positive sample bias (Stroscio and Celotta, 2004).
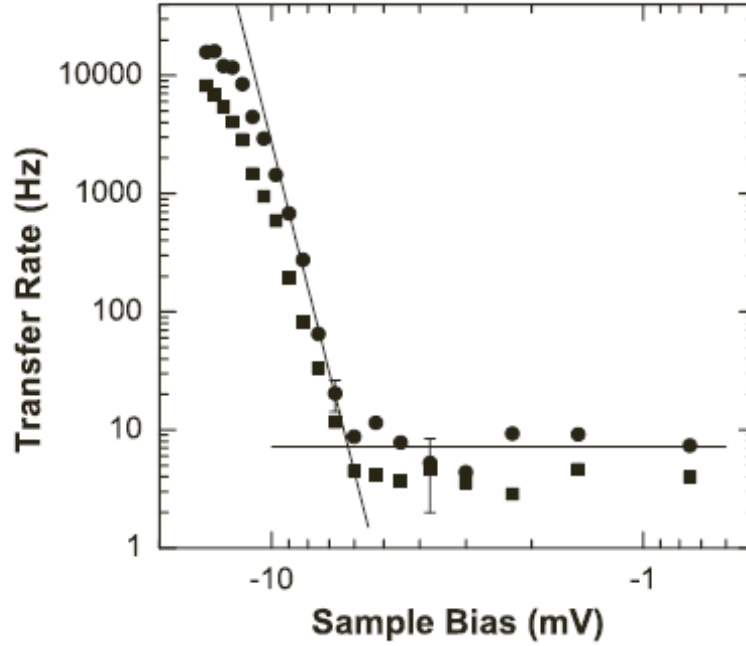

Figure 8. Transfer rate vs. sample bias at constant tip–Co atom height and negative sample bias obtained by measuring the distribution of residence time in the hcp and fcc sites from two-state random telegraph noise in the tunnel current. Tunneling resistance 150 kΩ, T = 2.3 K. Rate leaving hcp (fcc) site is depicted by circles (squares). Solid line shows a power law fit to initial threshold region and the horizontal line shows the average transfer rate for the low bias region, for the hcp transfer rate (Stroscio and Celotta, 2004).

To understand the rapid variation of transition rate with sample bias, or equivalently tunneling current in these fixed tip height measurements, we turn to theory (Gao et al., 1992; Gao et al., 1997; Walkup et al., 1993; Brandbyge and Hedegard, 1994) developed to explain a different atom manipulation experiment. Eigler and colleagues (1991) demonstrated that an adsorbed Xe atom on a Ni(110) surface could be transferred reversibly from the surface to the tip by pulsing the bias voltage. A portion of their data also exhibited a strong dependence of transition rate on tunneling current, varying with

the approximately 4.9[th] power of the current. In our work, the part of the transition rate

data shown in Figure 8 that varies rapidly with tunneling current can be understood by

considering the vibrational states shown in Figure 5C for the fcc and hcp binding sites.

Figure 5C depicts schematically the case where the tip is positioned above the hcp site

and the tip-adatom potential has deepened the potential at the hcp site and presumably

lowered the tunneling barrier between sites. At the 2.3 to 4.3K sample temperatures

used, the probability of a Co atom surmounting the tunneling barrier would be minuscule.

However, vibrational excitation is possible via inelastic scattering of the tunneling

electrons and, if the vibrational lifetime is sufficiently long, a series of vibrational

excitations can drive the adatom to a vibrational level at the top of the potential barrier.

As the probability of each excitation through inelastic electron scattering depends on the

occupancy of the lower vibrational level, the probability of atom transfer is proportional

to the tunneling current to the power n, where n is the number of the vibrational level

corresponding to the top of the barrier. For the region just above the onset of the rapid

increase in the hcp transition rate, i.e., from -7 to -9 mV, the data are well described by a

power law with an exponent of 12.5 ± 1.2. At higher currents, the transition rate appears

to saturate, possibly due to saturation of the first vibration transition.

The region between -0.5 and -5.0 mV shows no significant variation in transition rate

with bias voltage or tunneling current. We attribute this to atom tunneling through the

barrier between adjacent hcp and fcc sites. While it may seem highly unlikely that an

atom as heavy as Co could tunnel between adjacent binding sites, when each potential

well is of order 37 meV deep (Tsivlin et al., 2003), a simple calculation (Stroscio and

Celotta, 2004) demonstrates that this is reasonable. For an estimated barrier height of 37

meV and a tunneling barrier width of 0.75 Å, a transfer rate of about 30 Hz can be
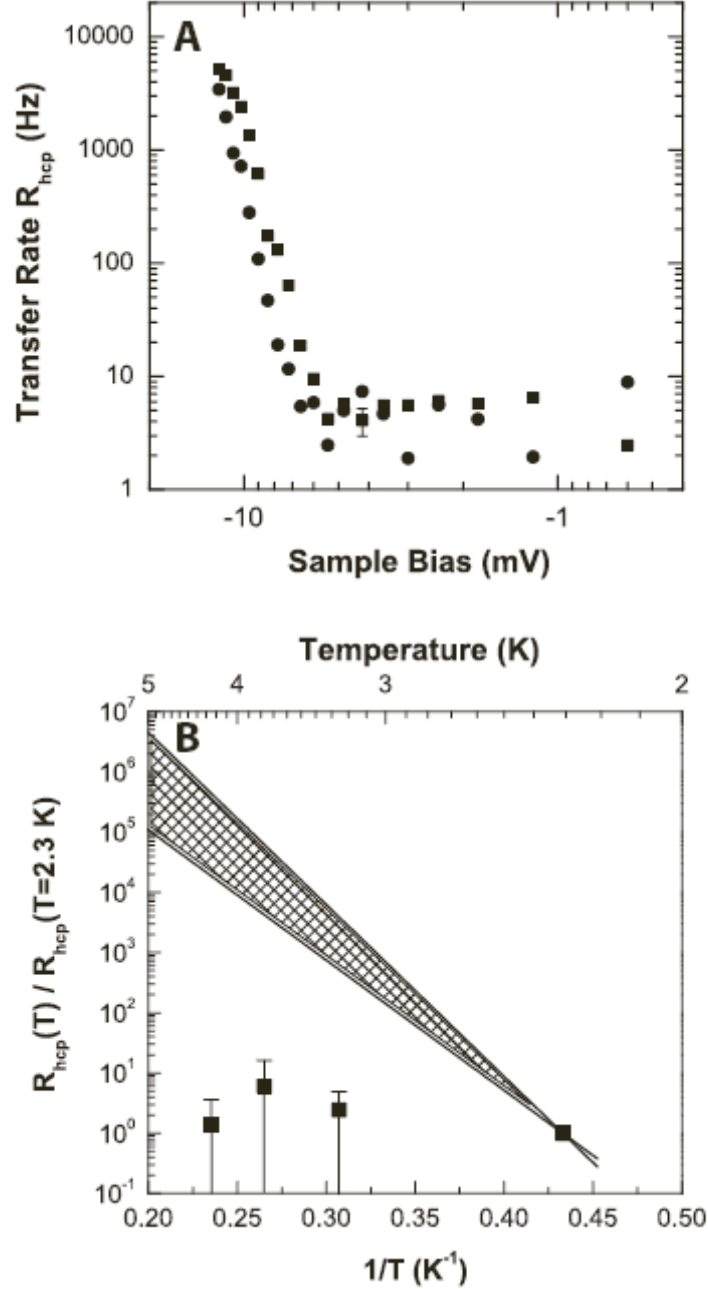

Figure 9. (A) Transfer rate leaving hcp site as a function of sample bias at 2.3 K (circles) and 4.3 K (squares) obtained from two-state telegraph noise near the hcp site. Junction resistance is 120 kΩ for both measurements. (B) Squares show ratio of the transfer rates leaving the hcp site at different temperatures to the transfer rate at 2.3 K (averaged for |sample bias| < 5 mV) vs. temperature; lines show arrhenius model for thermal activated transfer based on the rate observed at 2.3 K. Lower solid line is for a vibrational frequency of υ = 1010 Hz, upper solid line is for υ = 1013 Hz.

estimated using the WKB approximation (Landau et al., 1977). This is in reasonable

agreement with the observations within the range of sample bias where the transfer rate is

constant. However, thermally activated transitions could give rise to similar

observations. To rule out thermal excitation, the transition rates were measured as a

function of sample bias for two different temperatures, 2.3K and 4.3K, as shown in

Figure 9A. The curves for both temperatures are similar, each having a rapidly rising

feature, due to vibrational heating, and a flat region we believe is due to Co atom

tunneling. If thermally activation were responsible for the flat region, we would expect

the transition rates to depend exponentially on temperature. In Figure 9B we plot the

ratio of the transition rate for leaving the hcp site at four temperatures to the same rate at

2.3K. There does not appear to be any significant variation of this ratio with temperature.

For comparison, we indicate the variation that would be expected, for vibrational

frequencies between 10^{10} and 10^{13} Hz, were the thermal activation process responsible.

Hence, we conclude that we are observing direct atom tunneling in this current and bias

range.

IV. Summary and Comments

Since the first discovery that atoms can be manipulated using an STM, a great deal of

progress has been made and the possible opportunities for future research and

applications have greatly expanded. We have a better understanding of the mechanisms

involved and we are now able to sense directly the atom dynamics that accompanies atom

manipulation.

For the system we have discussed here, Co adatoms on a Cu(111) surface, we have found that the tip-adatom interaction constitutes a tunable chemical bond that can be thought of as creating a trapping potential on the surface directly beneath the tip. It is the force derived from this potential that causes the adatom to follow the tip's lateral path. Alternatively, one can think of this potential as modifying the unperturbed potential landscape created by the chemical bonding of the Co atom to the Cu lattice ion cores in such a way that the atom's local potential minimum is usually found just below the tip. Hence, the process is one of establishing a moving local potential minimum strong enough to move the atom from its favored binding site and narrow enough to constrain the atom dynamics so that the atom cannot access a second stable binding site when the tip is directly over a stable binding site. Vibrational excitation helps the atom surmount its local barrier to follow the moving local potential minimum. This is all possible owing to the extreme sensitivity to distance of both the tip-adatom interaction and the tunneling current and the extreme stability, sensitivity, and control of tip position possible in low-temperature scanning tunneling microscopy today. The strength of the trapping interaction required to accomplish atom manipulation can be tuned over many orders of magnitude by positioning the tip with sub-picometer precision and stability. The degree of vibrational excitation depends strongly on the tunneling current, in this particular case varying with the current to the 12.5^{th} power. The wide dynamic range of the interactions with the parameters we can control bodes well for the extension of this method of atom manipulation, with slight variations, to in a wide variety of systems and nanofabrication challenges.

V. Future Expectations

The ability to place atoms one-by-one, exactly where you want them turns a crystal surface into a veritable quantum workbench where the ramifications of electron coherence and confinement can be observed and their application to future devices can be tested. In many cases, small structures will be studied in great detail, exploring situations that might be very difficult to calculate, for example how a single or few atom defect would affect a device performance. However, there will be need for the construction of a variety of large collections of atoms as well. There are requirements for large sparse confinement structures, dense collections of atoms to probe, for example, the onset of ferromagnetism, and moderately dense nanostructures to probe the possibility of computation where spin information is communicated rather than charge being transported. Additionally, the exploration of this new uncharted territory may benefit substantially from an approach that accepts the fact that we do not a priori know all the answers. By using a combinatorial approach, involving the fabrication of a series of nanostructures for investigation, it may be possible to more quickly find the answer we are looking for, or even better, discover new phenomena that we never anticipated.

To reach its maximum potential, nanostructure fabrication via atom manipulation must be capable of operating on a variety of atoms and substrates, allow the assembly of 1-, 2-, and 3-dimensional nanostructures, and be relatively easy to accomplish. To this end, we have been working on the development of an Autonomous Atom Assembler (AAA) (to be published) which consists of an STM and a computer control system to allow the construction of desired nanostructures without human intervention starting from a

random collection of atoms and a schematic drawing of the desired structure. The AAA

computer program constitutes a continuously growing codification of such knowledge

about atom manipulation as has been presented above. The rules for manipulating

specific species are maintained within the AAA, as are rules pertaining to the interactions

between different atomic species. Using measurements similar to those of Hla et al., as

described above, it may prove feasible to have the AAA establish many of the rules by

itself. Presently capable of rapidly and autonomously assembling simple structures

composed of single Co atoms on a Cu(111) surface, the assembler is being generalized to

the simultaneous assembly of multiple species of atoms into a nanostructure. Eventually,

we expect its capabilities will be extended to three-dimensional construction and

semiconductor substrates.

The discussion we presented here has focused on the use of an STM to perform

nanofabrication atom-by-atom. However, a quite different perspective is also possible.

One can think of the atom moving across the surface while trapped under the STM tip as

a measurement probe. Much as one used test charges as probes in illustrations in physics

texts, a neutral atom scanned at very close range over a nanostructure will respond to its

local environment. In the work described here, the Co atom's dynamics was a

consequence of bond making and breaking as the atom probed each part of the Cu(111)

surface. The Co atom served as a single atom probe of surface binding sites. The STM

acted as a nanopositioning device and, by means of its tunneling current measurement, as

a nanotransducer of the single Co atom's response to binding site variations on the

nanoscale. We use the term Atom Based Metrology to refer to the method of scanning a

single trapped atom while monitoring its response to its environment in order to perform measurements on the nanoscale. One can imagine that, using a variety of transducers, single atom measurements of such nanoscale properties as electric and magnetic fields could be possible.

Acknowledgements

References

Avouris, P. (1995). Manipulation of matter at the atomic and molecular levels. *Accounts of Chemical Research* **28**, 95-102.

Bartels, L., Meyer, G., and Rieder, K. H. (1997). Basic steps of lateral manipulation of single atoms and diatomic clusters with a scanning tunneling microscope tip. *Physical Review Letters* **79**, 697-700.

Binnig, G., Rohrer, H., Gerber, C., and Weibel, E. (1983). 7X7 Reconstruction on Si(111) resolved in real space. *Physical Review Letters* **50**, 120-123.

Brandbyge, M., and Hedegard, P. (1994). Theory of the Eigler switch. *Physical Review Letters* **72**, 2919-2922.

Crommie, M. F., Lutz, C. P., and Eigler, D. M. (1993). Confinement of electrons to quantum corrals on a metal-surface. *Science* **262**, 218-220.

Eigler, D. M., and Schweizer, E. K. (1990). Positioning single atoms with a scanning tunneling microscope. *Nature* **344**, 524-526.

Eigler, D. M., Lutz, C. P., and Rudge, W. E. (1991). An atomic switch realized with the scanning tunneling microscope. *Nature* **352**, 600-603.

Feynman, R. P. (1960). There's plenty of room at the bottom. *Engineering and Science* **23**, 22-36.

Gao, S. W., Persson, M., and Lundqvist, B. I. (1992). Atomic switch proves importance of electron-hole pair mechanism in processes on metal-surfaces. *Solid State Communications* **84**, 271-273.

Gao, S. W., Persson, M., and Lundqvist, B. I. (1997). Theory of atom transfer with a scanning tunneling microscope. *Physical Review B* **55**, 4825-4836.

Gimzewski, J. K., and Joachim, C. (1999). Nanoscale science of single molecules using local probes. *Science* **283**, 1683-1688.

Hla, S. W., Braun, K. F., and Rieder, K. H. (2003). Single-atom manipulation mechanisms during a quantum corral construction. *Physical Review B* **67**, 1402-1404.

Ho, W. (2002). Single-molecule chemistry. *Journal of Chemical Physics* **117**, 11033-11061.

Kuhnle, A., Meyer, G., Hla, S. W., and Rieder, K. H. (2002). Understanding atom movement during lateral manipulation with the STM tip using a simple simulation method. *Surface Science* **499**, 15-23.

Landau, L. D., and Liftshitz, E. M. (1977). "Quantum Mechanics." Pergamon, New York.
Manoharan, H. C., Lutz, C. P., and Eigler, D. M. (2000). Quantum mirages formed by coherent projection of electronic structure. *Science* **403**, 512-515.

Levine, J., Celotta, R. J., and Bederson, B. (1968). Measurement of the electric dipole polarizabilities of metastable mercury. *Physical Review* **171**, 31-35.

Stipe, B. C., Rezaei, M. A., and Ho, W. (1998). Inducing and viewing the rotational motion of a single molecule. *Science* **279**, 1907-1909.

Stroscio, J. A., and Eigler, D. M. (1991). Atomic and molecular manipulation with the scanning tunneling microscope. *Science* **254**, 1319-1326.

Stroscio, J. A., Pierce, D. T., Dragoset, R., A., and First, P. N. (1992). Microscopic aspects of the initial growth of metastable fcc-iron on Au(111). *Journal of Vacuum*

Science and Technology A **10**, 1981-1985.

Stroscio, J. A., and Kaiser, W. J. (1993). "Scanning Tunneling Microscopy", Methods of Experimental Physics 27, Academic Press, San Diego.

Stroscio, J. A., and Celotta, R. J. (2004). Controlling the dynamics of a single atom in lateral atom manipulation. *Science* **306**, 242-247.

Tsivlin, D.V., Stepanyuk, V.S., Hergert, W., and Kirschner, J. (2003). Effect of mesoscopic relaxations on diffusion of Co adatoms on Cu(111), *Physical Review B* **68**, 205411-4.

Walkup, R. E., Newns, D. M., and Avouris, P. (1993). Role of multiple inelastic transitions in atom-transfer with the scanning tunneling microscope. *Physical Review B* **48**, 1858-1861.

Weissman, M. B. (1988). 1/F noise and other slow, nonexponential kinetics in condensed matter. *Reviews of Modern Physics* **60**, 537-571.

Whitman, L. J., Stroscio, J. A., Dragoset, R. A., and Celotta, R. J. (1991). Manipulation of adsorbed atoms and creation of new structures on room-temperature surfaces with a scanning tunneling microscope. *Science* **251**, 1206-1210.